Comparison of Transcript and Protein Abundance in Human Donor Retinas Support Extending Postmortem Interval From 12 to 18 Hours to Expand the Donor Pool for Biomedical Research

Cerys A. Easton,[1] Phillip A. Wilmarth,[2] Megan Criss,[3] Kilsun Kim,[2] Ashok P. Reddy,[2] Sophia Tanne,[1] Jason Q. Boone,[3] and Khoa D. Tran[1]

[1]Mark A. Terry, M.D. Research Laboratory, VisionGift, Portland, Oregon, United States
[2]Proteomics Shared Resource, Oregon Health and Science University, Portland, Oregon, United States
[3]Floragenex, Inc., Beaverton, Oregon, United States

Correspondence: Khoa D. Tran, VisionGift, 2201 SE 11th Ave., Portland, OR 97214, USA; khoa@visiongift.org.

Received: October 6, 2025
Accepted: March 10, 2026
Published: April 3, 2026

Citation: Easton CA, Wilmarth PA, Criss M, et al. Comparison of transcript and protein abundance in human donor retinas support extending postmortem interval from 12 to 18 hours to expand the donor pool for biomedical research. *Invest Ophthalmol Vis Sci.* 2026;67(4):9. https://doi.org/10.1167/iovs.67.4.9

Purpose. To evaluate whether extending the postmortem interval (PMI) from 12 to 18 hours affects transcript and protein abundances in the human retina.

Methods. Donor eyes were recovered from postmortem donors ($n = 7$ pairs) and stored at 2°C–8°C. Only donor eyes with ocular cooling within eight hours of death were examined. The OD retina was preserved at 12 hours and the OS retina at 18 hours postmortem. Retinas were flash frozen with liquid nitrogen. The macular region superior to the fovea was used for RNA sequencing (RNA-seq), whereas the inferior region was processed for tandem mass tag (TMT) quantitative proteomics. RNA library preparations were performed simultaneously, and the sequencing of all samples were conducted on the same chip. Proteins were isolated and labeled with 16-plex TMTPro isobaric tags, and all samples were analyzed in a 20-fraction TMT-mass spectrometry experiment. RNA-seq data were processed using DESeq2 (Bioconductor) and proteomic data were analyzed using the previously published PAW pipeline.

Results. RNA-seq identified 22,446 transcripts, with only five transcripts showing significant differential expression (adjusted $P < 0.1$ and a Log2FoldChange > 1) between 12 and 18 hours. No enriched pathways were associated with these changes. Proteomic analysis identified 6,109 proteins, with no significant differences in abundance (all adjusted $P > 0.05$). Retinal cell-type specific markers and markers relevant for disease research, such as age-related macular degeneration and glaucoma, remained stable across both time points.

Conclusions. Extending the PMI cutoff from 12 to 18 hours did not significantly impact transcriptomic or proteomic integrity in human donor retinas. This PMI extension greatly increases the availability of donor eyes for biomedical research.

Keywords: postmortem interval, retina transcriptome, retina proteome, retina, eye banking

Unlike other human tissues that can be procured for biomedical research via surgical biopsy, the retina must be obtained postmortem, necessitating collaboration with eye banks or other tissue procurement agencies. Researchers studying retinal diseases are increasingly requesting human donor retina with short postmortem intervals (PMI), typically defined as the time between the donor's death and final tissue preservation, often within 12 hours of donor death. Although eye banks actively support ocular research, legal and logistical constraints, such as transporting tissues back to the laboratory for preservation, can result in PMIs extending beyond the preferred time frame.[1]

Many researchers set current PMI restrictions based on studies in animal models demonstrating increased RNA and protein degradation with longer PMIs. However, these findings are inconsistent and vary depending on species, tissue handling, and storage conditions.[2–9] For example, a study on mice and baboon retinas found increased RNA degradation with longer PMIs, but the enucleated eyes were stored at room temperature for the duration of the experiment.[2] In contrast, porcine eyes stored under refrigeration in humidified chambers, consistent with eye banking protocols, resulted in retinal RNA that were stable for up to 48 hours postmortem.[3,10]

There are substantial structural and cellular differences between the human retina and those of commonly used animal models that complicate direct comparisons. These differences include the differences of the fovea centralis,[11,12] the lack of a true macula in mice,[13,14] and species-specific variations in the abundance and distribution of photore-

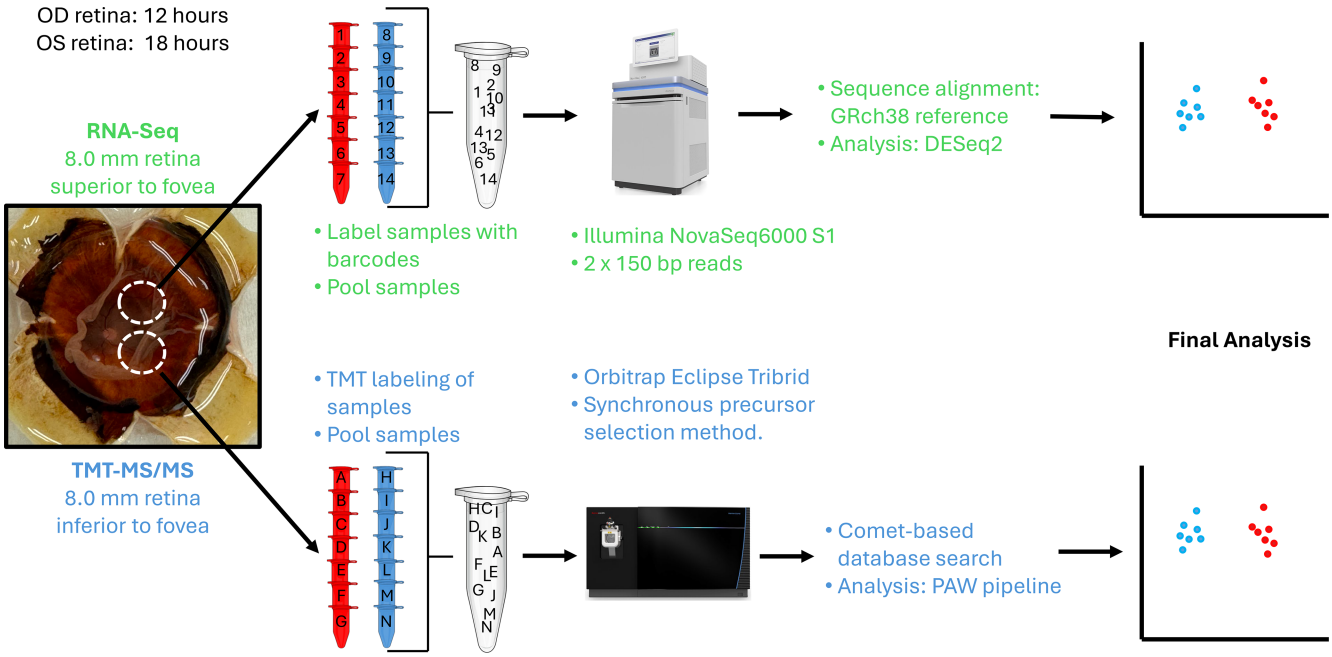

Figure 1. Methods and analysis techniques. Donor whole eyes or poles were recovered from postmortem donors ($n = 7$ pairs) and stored at 2°C–8°C. Tissues were dissected, and two 8.0 mm diameter retina punches were taken, the OD retina punches were frozen at 12 hours, and the OS retina punches were frozen at 18 hours postmortem. The punch above the fovea was designated for RNA sequencing (transcriptome) analysis and the punch below the fovea was designated for tandem mass tag (TMT)-mass spectrometry (proteome) analysis. Analogous techniques were used for transcriptome and proteome analysis: RNA sequencing of all donor samples was conducted on the same chip using specific barcode tags for each respective donor, and mass analysis of all donor protein samples was analyzed in a single TMT-mass spectrometry experiment using specific TMTPro isobaric tags for each respective donor. RNA-seq data were processed using DESeq2 (Bioconductor) and proteomic data were analyzed using the PAW pipeline.[20]

ceptors and other retinal cell types, even among nonhuman primates.[15–17] Consequently, the applicability of animal model data to human retinal tissue is limited, and the optimal PMI range for human retina remains uncertain.

Our literature review identified a lack of systematic studies on human retinal tissue stability under eye bank conditions. To address this gap, we examined the transcript and protein abundance in the human retina at 12 and 18 hours postmortem. The 12-hour PMI represents a compromise between the scientific preference for minimal degradation and the practical realities of tissue donation. Our findings suggest that extending the upper limit of PMI from 12 to 18 hours could increase donor tissue availability by approximately 92%, based on data presented in our previous report.[1]

Methods

Donor Characteristics

Donor eye tissues were recovered with legal authorization for donation by the legal next of kin in accordance with the Uniform Anatomical Gift Act. Eyes were placed in moist chambers (jars containing cotton soaked with sterile-BSS) and kept at 2°C–8°C until retina preservation took place at 12 or 18 hours postmortem.

Tissue Preservation

Tissue dissections were performed under a microscope at VisionGift (Portland, OR, USA). For recovered whole eyes, the cornea was excised according to our eye bank's standard operating procedures. For recovery of posterior parts, aseptic excision of the cornea was performed in field, and the posterior parts containing the iris and all eye tissues posterior to it, were also placed into moist chambers for storage and transport. To isolate the retina, the iris and lens were removed, and the remaining retina, choroid, and scleral complex was cut at 3-, 6-, 9-, and 12-o'clock positions. The vitreous was carefully dissected away from the retina.

Preservation of retina tissues for downstream analysis is outlined in Figure 1. Two 8-mm punches were taken from the retina, one above the fovea (used for RNA-seq analysis) and one below the fovea (used for proteomics analysis). Retina samples for the oculus dexter (OD) eye were flash frozen with liquid nitrogen at 12 hours postmortem, and this process was repeated for the oculus sinister (OS) eye at 18 hours postmortem. All retina samples were stored at −80°C until they were processed for RNA-seq or tandem mass tag (TMT)-mass spectrometry.

RNA Extraction and Sequencing

RNA was extracted from each retina sample using the Zymo Direct-Zol RNA kit (cat no.: R2053; Zymo Research, Irvine, CA, USA) as per the manufacturer's instructions. Specifically, cell samples were lysed in TRI Reagent and incubated for one hour at room temperature, followed by centrifugation to remove debris. After ethanol addition, RNA was bound to Zymo-Spin IICR columns (Zymo Research), washed with RNA Wash Buffer, and eluted with DNase/RNase-Free Water. RNA samples were analyzed using an Agilent 5200 Frag-

Investigative Ophthalmology & Visual Science

Table 1. Donor and Tissue Characteristics

Donor	Donor ID	Age	DtoC	DtoR	Tissue Recovered	Cause of Death	Ethnicity	RIN 12-Hour	RIN 18-Hour
D1	24-0686	80	1:07	8:26	Whole eyes	Septic shock	C	6.2	6.4
D2	24-0722	80	2:23	3:24	Whole eyes	Respiratory failure	C	6.3	5.9
D3	24-1108	77	1:58	4:03	Whole eyes	Pancreatic cancer	C	4.8	5.0
D4	24-1259	64	2:11	5:06	Whole eyes	Respiratory failure	C	6.3	6.8
D5	24-1287	77	2:22	5:24	Whole eyes	Dementia	C	6.1	4.4
D6	24-1408	47	2:36	3:43	Posterior Poles	Anoxic brain injury	C	6.7	4.4
D7	24-1432	75	6:20	11:10	Posterior Poles	Respiratory failure	C	5.3	5.8
	Avg ± SD	71 ± 11	2:42 ± 1:32	5:53 ± 2:39					

C, Caucasian; DtoC, death-to-cooling; DtoR, death-to-recovery; RIN, RNA integrity number.

DtoC is time between donor death and initiation of cooling of the eyes with wet ice or cooling of the whole body. DtoR is the time between donor death to eye tissue recovery. After recovery, the whole eyes or poles are kept in a moist chamber at 2°C–8°C until retina preservation. Eyes from seven donors were procured for this work.

ment Analyzer (Agilent Technologies, Winooski, VT, USA) and reported in Table 1 for all samples.

Library Preparation and Sequencing

Total RNA samples were subjected to library preparation using the Watchmaker RNA Kit with Polaris Depletion (cat no.: 7BK0002; Watchmaker Genomics, Boulder, CO, USA) as per the manufacturer's instructions to remove ribosomal RNA. The Polaris Depletion reactions were performed at full scale, and the library preparation reactions were performed at half scale. RNA fragmentation, first-strand cDNA synthesis, second-strand synthesis, A-tailing, and adapter ligation were performed following the kit's instructions. The libraries were amplified, and a post-ligation cleanup was applied using SPRI beads (Beckman Coulter, Inc, Southfield, MI, USA). The final libraries were sequenced on the Illumina NovaSeq6000 S1 300 (Illumina, San Diego, CA, USA) Cycle in 2 × 150 bp fashion, producing between 46.8 and 80.5 million reads per sample.

Quality Validation, Trimming, and Read Alignment

Quality of sequence reads was evaluated using FastQC to assess the overall quality and sequence composition. Cutadapt was used to separate reads with adapters from the reads without adapters. The reads with no adapter contamination were further processed using Trimmomatic to validate read pairs and to remove low-quality reads, based on predefined thresholds of LEADING:30, TRAILING:30, and MINLEN:101. Quality of trimmed reads was re-validated using FastQC. Final libraries contained between 25.9 and 33.7 million reads per sample.

The cleaned reads were aligned to the human GRCh38 (GENCODE v32/Ensembl 98) reference genome using the splice-aware aligner STAR. The STAR alignment was carried out with default settings, and the resulting BAM files were processed using HTSeq-count to quantify transcript counts and generate count tables from the aligned reads for each sample.

Data Transformation and Downstream Analysis

The HTSeq-count tables were imported into R for differential expression analysis using DESeq2.[18] First, a DESeq DataSet object was created from the count tables, specifying the experimental design and conditions. The dataset was filtered to retain genes with counts greater than one across all samples to reduce the size of the dataset.

Variance stabilizing transformations and rLog transformations were performed to normalize the data and stabilize the variance across samples. Both transformations were visualized through various plots to assess the relationships between the samples. Principal component analysis (PCA) was conducted to explore the variance between the samples, with the transformed data (variance stabilizing transformations and rLog) used to generate the PCA plots.

For differential expression analysis, DESeq2 was used to estimate size factors and perform the differential analysis using a Log_2Fold Change (Log_2FC) threshold. Differentially expressed transcripts were identified as those having an adjusted *P*-value (*P-adj*) < 0.1 and $Log_2FC > 1$. The results were further analyzed and visualized using ggplot2, including MA plots, heatmaps, and gene clustering to highlight the differentially expressed genes across the samples.

Meta-Analysis of Six- and 12-Hour Postmortem Samples

Bulk RNA-seq data previously reported for retinal samples with a six-hour PMI[19] were compared with our 12-hour PMI samples. Raw sequencing data were downloaded from the Gene Expression Omnibus (accession number GSE169046) and processed using the same analysis pipeline described above.

Protein Homogenization and Extraction

Frozen retina samples were suspended in 500 µL of 5% SDS, 50mM TEAB, then subject to bead beating for six 20-second cycles in a Precellys Evolution bead beater (Bertin Instruments, Montigny-le-Bretonneux, France) at 4°C. Samples were spun in a centrifuge at 8000*g* for five minutes at 4°C. The bead beating and centrifugation procedure was repeated once. Samples were heated to 90°C for 10 minutes in an Eppendorf Thermomixer C (Eppendorf, Hamburg, Germany), then spun in a centrifuge at 8000*g* for five minutes at 4°C. Samples were subject to ultrasonication for 40 minutes using a Covaris Evolution E220 ultrasonicator (Covaris, Woburn, MA, USA), then spun in a centrifuge for five minutes at 16,000*g*, and then stored at −80°C.

Investigative Ophthalmology & Visual Science

Table 2. RNA-Seq Normalized Counts and TMT Mass Spectrometry Normalized Intensity of Common Retinal Markers and Housekeeping Genes

		Transcriptomics					Proteomics				
			Normalized RNA Seq Counts					Normalized Spectral Intensity			
Cell Type	Gene Name	Gene Symbol	12-Hour Average	18-Hour Average	Log2FC	Adj. *P*-Value	Protein Symbol	12-Hour Average	18-Hour Average	Log2FC	Adj. *P*-Value
Photoreceptor	Recoverin	*RCVRN*	23.47	26.16	<0.0001	**0.94**	RECO	26,845,128	25,915,900	−0.051	**0.999**
	Phosducin	*PDC*	22.90	23.65	<0.0001	**0.99**	PHOS	17,954,290	16,698,544	−0.093	**0.999**
	Rhodopsin	*RHO*	28.74	32.36	<0.0001	**0.90**	OPSD	40,905,978	44,700,155	0.128	**0.999**
Horizontal cells	Calbindin	*CALB1*	18.79	17.97	<0.0001	**0.97**	CALB1	3,259,793	3,079,026	−0.082	**0.999**
Bipolar cells	Visual system homeobox 2	*VSX2*	2.90	1.25	<0.0001	**0.47**	VSX2	853,279	857,891	0.015	**0.999**
	Transient receptor potential cation channel subfamily M member 1	*TRPM1*	1.10	2.01	<0.0001	**0.83**	TRPM1	99,772	100,218	0.003	**0.999**
Amacrine cells	Paired box 6	*PAX6*	100.03	97.82	<0.0001	**0.97**	PAX6	49,291	55,337	0.167	**0.999**
RGCs	RNA-binding protein with multiple splicing	*RBPMS*	147.24	150.00	<0.0001	**0.97**	RBPMS	76,753	77,979	0.023	**0.999**
	Calretinin	*CALB2*	0.76	0.13	<0.0001	**0.75**	CALB2	4,271,049	4,039,635	−0.080	**0.999**
Müller glia	Retinaldehyde-binding protein 1	*RLBP1*	1.75	1.38	<0.0001	**0.96**	RLBP1	40,172,107	36,810,717	−0.126	**0.999**
	Prospero-related homeobox 1	*PROX1*	77.56	63.54	<0.0001	**0.76**	PROX1	52,058	51,384	−0.019	**0.999**
Housekeeping genes (non-specific cells)	Glyceraldehyde-3-phosphate dehydrogenase	*GAPDH*	5.58	5.71	<0.0001	**0.99**	G3P	349,443,239	345,398,742	−0.017	**0.999**
	Peptidyl-prolyl cis-trans isomerase B	*PPIB*	1.08	0.29	<0.0001	**0.36**	PPIB	3,620,352	3,621,736	0.001	**0.999**
	Actin, cytoplasmic 1	*ACTB*	3.61	3.05	<0.0001	**0.96**	ACTB	22,756,920	23,027,917	0.017	**0.999**
	Tubulin beta chain	*TUBB*	0.38	0.0	<0.0001	**0.95**	TBB5	10,019,609	10,449,367	0.061	**0.999**

Gene names and corresponding gene symbols are shown with the average measurements for the 12- and 18-hour groups from the RNA-seq and mass spectrometry experiments. Log2 fold change (Log2FC) and associated adjusted *P*-values are also shown.

Table 3. RNA-Seq Normalized Counts and TMT Mass Spectrometry Normalized Intensity of Common Apoptosis Markers and Cellular Repair Genes

		Transcriptomics					Proteomics				
			Normalized RNA Seq Counts					Normalized Spectral Intensity			
Marker Type	Marker Name	Gene Symbol	12-Hour Average	18-Hour Average	Log2FC	Adj. *P*-Value	Protein Symbol	12-Hour Average	18-Hour Average	Log2FC	Adj. *P*-Value
Apoptosis markers	Caspase 3	*CASP3*	1.74	3.44	<0.0001	**0.37**	CASP3	278,467	265,248	−0.072	**0.999**
	Apoptosis inducing factor	*AIFM1*	1.08	0.56	<0.0001	**0.74**	AIFM1	10,208,695	10,549,958	0.047	**0.999**
	Death domain-containing protein CRADD	*CRADD*	0.16	0.42	<0.0001	**0.96**	CRADD	65,451	63,482	−0.044	**0.999**
	Apoptosis-stimulating of p53 protein 2	*TP53BP2*	3.13	2.40	<0.0001	**0.88**	ASPP2	34,515	34,950	0.018	**0.999**
	Serine protease HTRA1	*HTRA1*	7.19	2.71	<0.0001	**0.03**	HTRA1	172,824	177,544	0.039	**0.999**
	Cytochrome c	*CYCS*	0.27	0.97	<0.0001	**0.49**	CYC	2,311,184	2,382,199	0.044	**0.999**
Cellular repair markers	Poly [ADP-ribose] polymerase	*PARP1*	2.13	0.29	<0.0001	**0.20**	PARP1	12,807,298	12,430,503	−0.043	**0.999**
	DNA-directed RNA polymerase II subunit RPB1	*POLR2A*	3.99	1.93	<0.0001	**0.31**	RPB1	1,473,969	1,464,814	−0.009	**0.999**
	Superoxide dismutase [Mn]	*SOD2*	101.57	83.27	<0.0001	**0.49**	SODM	9,360,729	9,842,892	0.072	**0.999**
	Phospholipid hydroperoxide glutathione peroxidase	*GPX4*	1.71	1.47	<0.0001	**0.97**	GPX4	3,538,208	3,526,659	−0.005	**0.999**
	DnaJ homolog subfamily B member 1 (HSP40)	*DNAJB1*	59.64	55.73	<0.0001	**0.96**	DNJB1	1,023,452	999,855	−0.057	**0.999**
	Heat shock 70 kDa protein 1A	*HSPA1A*	0	0	0.0	**1.0**	HS71A	16,189,808	15,993,964	−0.018	**0.999**

Gene names and corresponding gene symbols are shown with the average measurements for the 12- and 18-hour groups from the RNA-seq and mass spectrometry experiments. Log2 fold change (Log2FC) and associated adjusted *P*-values are also shown.

Protein Assay

Protein concentration was determined using a Pierce BCA protein assay kit (Pierce, Appleton, WI, USA). Absorbance measurements were taken with a BioTek Epoch Microplate Spectrophotometer (Agilent BioTek, Santa Clara, CA, USA) at 562 nm. Once concentration was determined, 50 µg of protein was taken from each sample for S-trap digestion.

S-Trap Micro Digestion

Dithiothreitol was added to each sample to achieve a final concentration of 22 mM, then samples were incubated for 10 minutes at 95°C. Iodoacetamide was added to each sample to achieve a final concentration of 40 mM and samples incubated at room temp in the dark for 30 minutes. Phosphoric acid was added to each sample to achieve a final concentration of 1.2% phosphoric acid. Six times the sample volume of S-Trap protein binding buffer (90% aqueous methanol containing 100 mM TEAB, pH 7.5) was added to each sample.

Small portions of each sample were added to individual S-Trap micro columns and columns were spun in a centrifuge for three minutes at 4000*g*. This process was repeated until all sample volumes eluted from the column. Captured protein was washed six times by adding 150 µL of S-Trap protein binding buffer and spinning in a centrifuge at 4000*g* for three minutes. The digestion buffer (80 ng/L trypsin in 50 mM TEAB) was added (1:16 enzyme/substrate ratio) to the top of each column and incubated overnight at 37°C.

The peptide digests were eluted with 50 mM TEAB followed by 0.2% aqueous formic acid. The elutions were spun in a centrifuge at 4000*g* for four minutes. Hydrophobic peptides were eluted with 40 µL of 50% acetonitrile containing 0.2% formic acid. Eluted peptides from individual samples were pooled and dried down in a Thermo Savant Speedvac (Thermo Fisher Scientific, Waltham, MA, USA) at room temperature.

Peptide Assay

Samples were resuspended in 100 µL of HPLC grade water, shaken at 37°C for 15 minutes, and spun in a centrifuge at 12,000*g* for five minutes. A Pierce Peptide Assay Kit was used to determine the concentration of peptide digests. Absorbance measurements were taken with a BioTek Epoch Microplate Spectrophotometer at 480 nm. Peptide digest aliquots of 15 µg from each sample was taken for TMTpro (Thermo Fisher Scientific) 16-plex labeling.

TMT Labeling and Multiplexing

Dried samples were dissolved in 20 µL of 100 mM TEAB (pH 8), shaken at 37°C for 10 minutes, and then spun in a centrifuge for five minutes at 14,000*g*. A solution of anhydrous acetonitrile and TMTpro labeling reagent was vortexed and spun in a centrifuge for five minutes at 14,000*g*. Label (12 µL) was added to each sample, shaken at room temperature at 850 rpm for one hour and spun in a centrifuge for five minutes at 14,000*g*.

From each sample, 2 µL was pooled and 2 µL of 5% hydroxylamine was added to create a TMT equal-volume-per-sample mixture. This mixture was dried and then resuspended in 5% formic acid for mass spectrometry analysis

using a 140-minute method. Multiplexing adjustment factors were calculated to equalize the sum of reporter ion signals per sample in the 35 µg final mixture, and volumes taken from each labeled sample were determined by the equal-intensity adjustment factors.

Hydroxylamine was added to the final pooled sample mixture such that the concentration was 0.5%. The mixture was dried, and 10.0 mM ammonium formate was added. The mixture was fractionated by a Dionex NCS-3500RS UltiMate RSLCnano UPLC (Thermo Fisher Scientific) into 20 fractions (online high pH 17% to 90% acetonitrile step elutions). Eluted fractions were separated with 140-min low-pH reverse phase chromatography and analyzed by an Orbitrap Eclipse Tribrid (Thermo Fisher Scientific) with survey scans performed in the Orbitrap (resolution 120K), and data-dependent MS2 scans in the linear ion trap using CID. Reporter ion detection was performed in the Orbitrap using MS3 scans (resolution 50K) after synchronous precursor isolation in the linear ion trap, and HCD in the instrument's ion-routing multipole.

Proteomic Data Analysis

Raw mass spectrometry files were analyzed using the PAW pipeline.[20] Comet (version 2016.3) searches were performed against a UniProt canonical human FASTA database (one protein per gene UP000005640 downloaded April 2024 with 20,598 protein sequences) with common contaminants and sequence-reversed decoys added.[21] Search parameters were 1.25 Da monoisotopic peptide mass tolerance, 1.0005 Da monoisotopic fragment ion tolerance, semi tryptic cleavage with up to three missed cleavages, variable oxidation of methionine residues, static alkylation of cysteines, and static modifications for TMTpro labels (at peptide N-termini and lysine residues).

The target/decoy method was used to filter peptide spectrum matches to a 1% false discovery rate (FDR). Parsimonious protein inference was used with a protein identification requirement of at least two distinct peptides per protein. Contaminants (keratins) were removed from the MS data. TMT reporter ion intensities were summed from all scans associated with unique peptides to produce total protein intensity values. Protein intensity values were normalized using the trimmed mean of M-values (TMM) normalization method[22] and statistical testing was done with the Bioconductor package edgeR.[23] Pairwise comparisons used the exact test with Benjamini-Hochberg multiple testing corrections.

Results

Donor and Tissue Characteristics

Eight pairs of donor retinas were originally collected and sent for sequencing and mass spectrometry. It was later discovered that one donor (the only female in the group) had active metastatic cancer at the time of death and had received chemotherapy within three months before death. Because chemotherapy could introduce retina-specific changes,[24] samples from this donor were excluded from our analysis to minimize variation unrelated to PMI. Of the seven remaining donors, five pairs of whole globes and two pairs of posterior segments were recovered, all from male donors. The average donor age was 71 ± 11 years (range 47 years to 80 years). The average death to time of ocular cooling was 2:42 ± 1:32 (hh:mm; range 1:07–6:20), and average time of death to eye recovery was 5:53 ± 2:39 (range 3:24 to 11:10). Donor age, death-to-cooling, death-to-recovery, the type of tissue recovered, and the cause of death for each donor are presented in Table 1.

Transcriptome Analysis

Average RNA integrity numbers for the 12-hour cohort were 5.9 (range 4.8 to 6.7) compared to the 18-hour cohort which were 5.6 (range: 4.4 to 6.8). The RNA-seq analysis yielded 42,243 unique RNA transcripts that include coding, non-coding, microRNAs, and novel transcripts (Supplementary Table S1). Of the total transcripts, 22,446 transcripts were annotated in the GRCh38 reference genome. In the pairwise comparison of all donors at 12-hour PMI, correlation of transcript abundance was high across all samples ($r^2 \geq 0.96$, Fig. 2A). Comparison of transcript counts between the 12- and 18-hour samples also showed high similarity between the two cohorts ($r^2 = 0.999$, Fig. 2B; Tables 2, 3).

The transcriptomic PCA analysis based on the top 500 transcripts by variance shows clustering of samples based on donors rather than on time of tissue preservation (Fig. 3A). There is no distinct separation of the 12- and 18-hour cohorts. The transcriptomic MA analysis shows 766 transcripts with significant changes (*P-adj* < 0.1, Fig. 3B); however, only five (two downregulated and three upregulated) had a $Log_2FC > 1$ (Fig. 3C). There was no enrichment of any specific pathways among those five genes. Subsequent proteomics analysis (below) confirm the lack of pathway enrichment (Figs. 4, 5).

Approximately 40% of all transcripts in our RNA-seq study had a basemean value of one or less, near the detection limit of the method, at the 12-hour PMI. Previous studies have reported median half-lives of ~9 hours for mammalian mRNAs and 5.1 hours for lncRNAs.[25,26] To investigate the potential changes before the 12-hour cutoff, we performed a meta-analysis comparing a published dataset of retina samples with a six-hour PMI with our 12-hour samples.[19] Principal component analysis showed clear separation between the two cohorts (Fig. 6A) and identified 14,580 differentially expressed transcripts (Fig. 6B; Supplementary Table S3). Of these, 5091 annotated transcripts showed a significant decrease in abundance, whereas 1969 were more abundant at 12 hours compared with six hours postmortem.

The PANTHER overrepresentation test (Version 19.0, released 2024-08-07)[27,28] performed on all annotated genes that were significantly reduced at 12 hours revealed significant enrichment for pathways related to light stimulus response and retinal homeostasis (~2.5-fold, FDR < 0.05). Consistent with this PANTHER analysis, photoreceptor markers *RCVRN*, *RHO, PDC,* and *ARR3*[29] and the ganglion cell marker *RBPMS*[30] were significantly less abundant at 12 hours postmortem, whereas markers for horizontal cells, bipolar cells, amacrine cells, and Müller glia remained stable (Fig. 6C). Thus changes in retinal cell-identity markers appear to be selective, suggesting differential changes in retinal cell types during this postmortem interval.

Overrepresentation test of genes that were more abundant at 12 hours revealed significant enrichment for pathways involved in DNA repair and regulation of cellular stress responses (>2-fold, FDR < 0.05). Within a targeted panel of apoptosis and cellular repair genes, *HTRA1* decreased, whereas canonical apoptosis markers (e.g., *BCL2*, *BAX*,

Investigative Ophthalmology & Visual Science

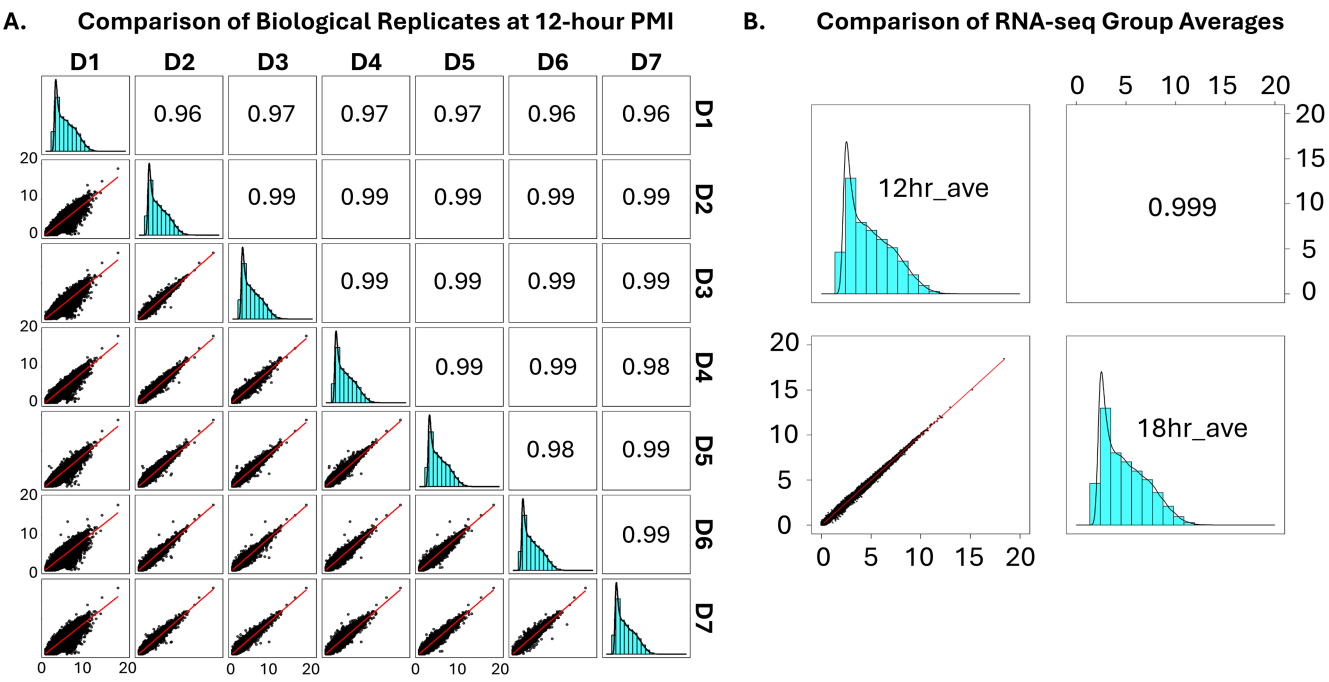

Figure 2. Transcriptome analysis results. **(A)** Scatter plot grid pair-wise comparisons of normalized RNA sequence counts for each of the 12-hour retinal samples. **(B)** Scatter plot of averaged normalized RNA sequence count values for all 12-hour samples compared to 18-hour samples.

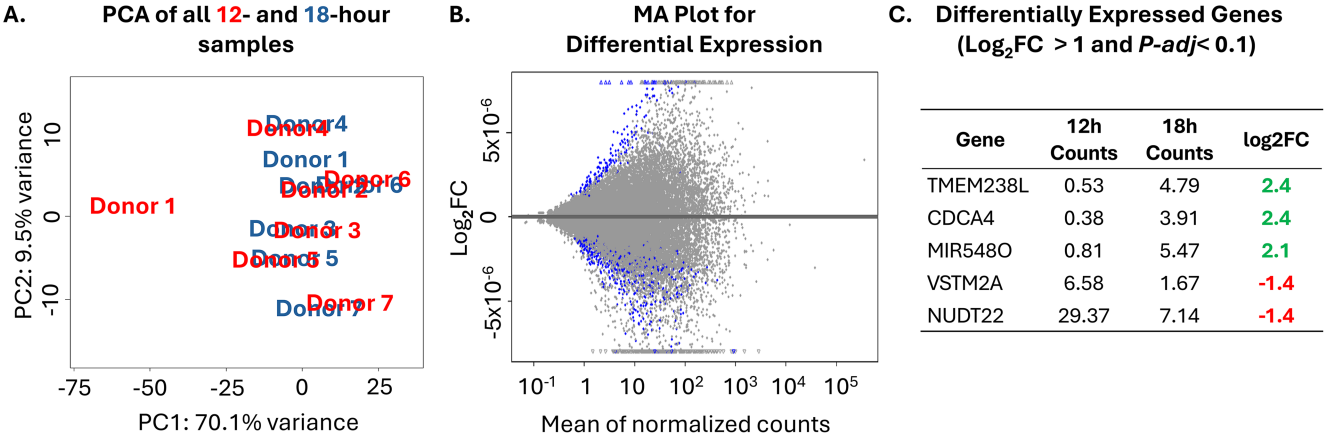

Gene	12h Counts	18h Counts	log2FC
TMEM238L	0.53	4.79	2.4
CDCA4	0.38	3.91	2.4
MIR548O	0.81	5.47	2.1
VSTM2A	6.58	1.67	-1.4
NUDT22	29.37	7.14	-1.4

Figure 3. Differential expression analysis. **(A)** Principal component analysis of all RNA Seq samples. *Red* = 12-hours, *Blue* = 18-hours. Donors tend to cluster more closely based on their respective tissue donor rather than on time. **(B)** MA plot for differentially expressed transcripts. *Blue dots* represent 473 genes with adjusted $P < 0.1$. **(C)** Table summarizing the five differentially expressed genes with Log2FC > 1 and adjusted $P < 0.1$.

CYCS, *CASP3*, *PARP1*) remained stable (Fig. 6C). Similarly, among housekeeping genes, *ACTB* declined while *GAPDH*, *PPIB*, and *TUBB* remained unchanged. Taken together, these results indicate that early postmortem transcriptomic changes reflect selective cellular vulnerability and active stress-response signaling, rather than passive RNA degradation and uniform stress response (see Discussion).

Proteome Analysis

The mass spectrometry analysis yielded 487,693 acquired MS2 scans. Of these, 159,894 scans were successfully identified (using a 1% FDR) by the Comet/PAW pipeline representing a 32.8% identification rate. The resulting peptide sequences mapped to 6224 unique proteins. After removing 63 decoy sequences and contaminant matches (e.g., keratins), as well as 52 proteins below the limit of quantification, a total of 6109 unique proteins were quantifiable (Supplementary Table S2).

Similar to the transcriptomic analysis, pairwise comparison of TMM-normalized signal between the seven biological replicates at 12-hours postmortem show high levels of similarity in the retinal proteomes ($r^2 \geq 0.99$, Fig. 4A). Comparison of protein abundance between the 12- and 18-hour cohorts indicate minimal differences ($r^2 \geq 1.00$, Fig. 4B, Tables 2, 3), suggesting there were no changes in protein abundance in the additional six hours of storage over the full range of spectral intensities (Fig. 5B).

Investigative Ophthalmology & Visual Science

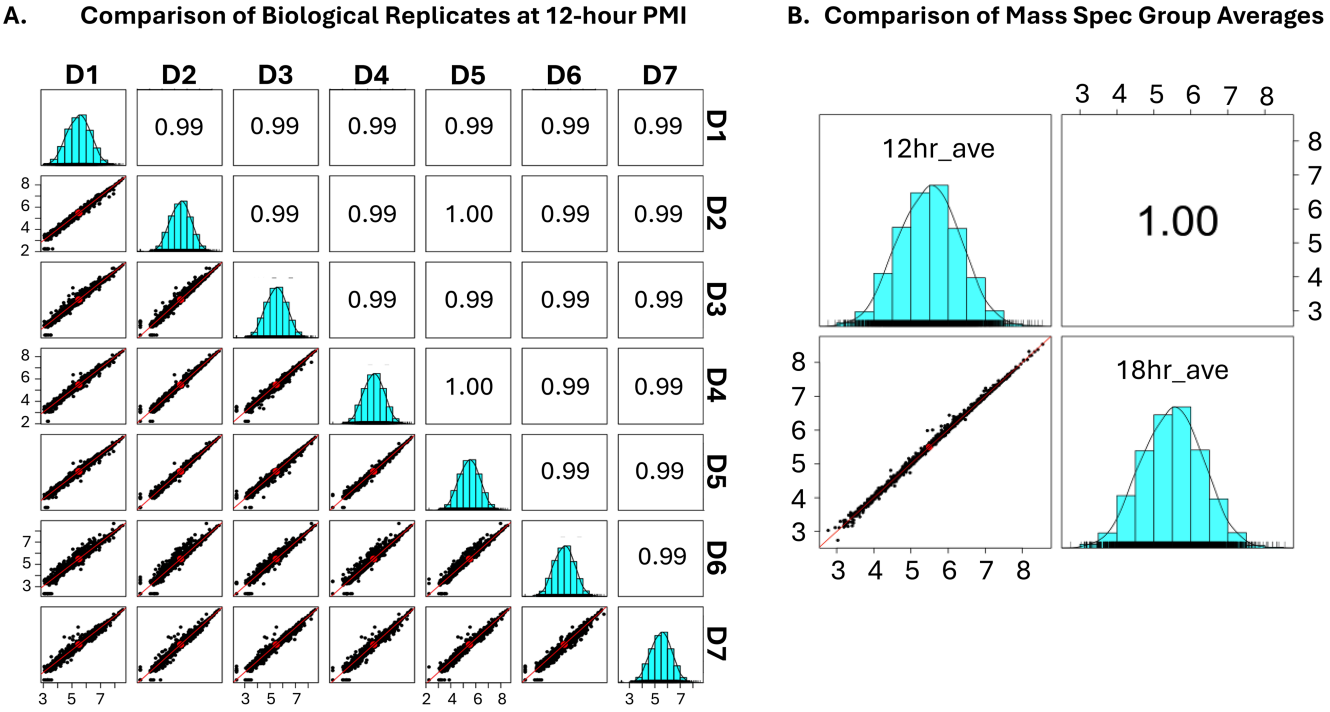

Figure 4. Proteomic analysis results. **(A)** Scatter plot grid with pair-wise comparison of each of the 12-hour retinal sample proteomes. Axis labels are TMM-normalized intensities (log10). **(B)** Scatter plot of averaged values for all 12-hour PMI samples compared to 18-hour PMI samples.

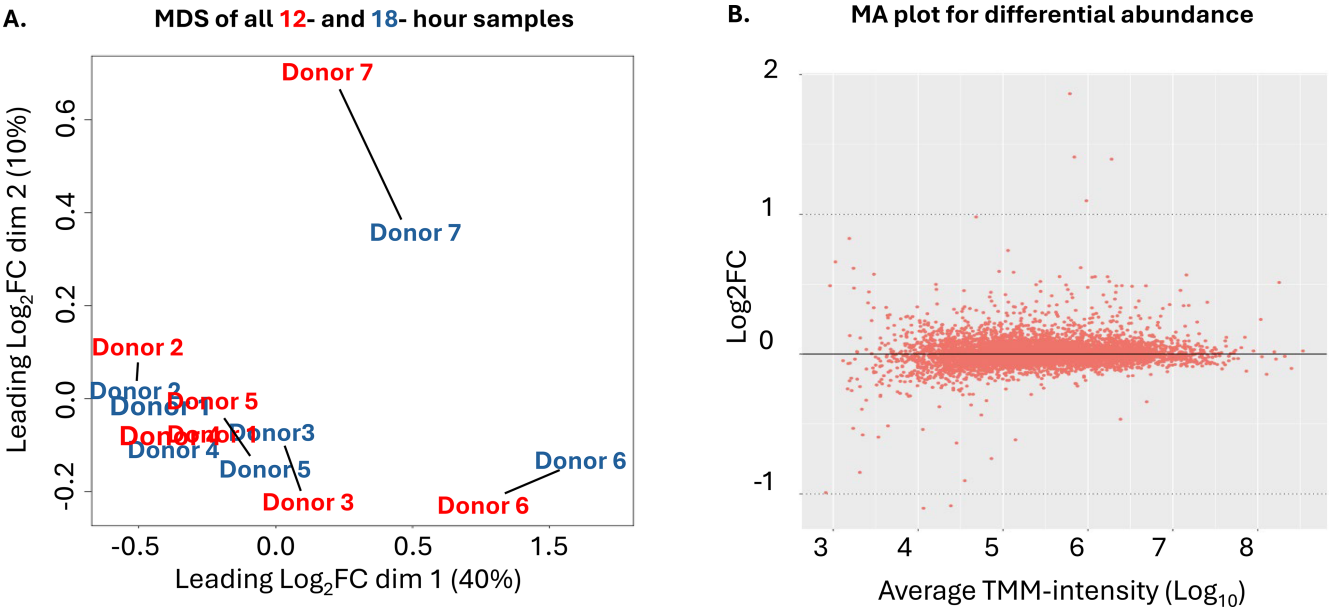

Figure 5. Differential protein abundance analysis. **(A)** Multidimensional scaling (MDS) plot. Axes show dimensions based on the leading Log2FC changes of the 500 proteins having the largest variation over the 14 samples. *Red* = 12-hour PMI, *Blue* = 18-hour PMI. **(B)** MA plot for all valid quantifiable proteins. *Solid black lines* in each plot indicate a one-to-one relationship, and *dotted lines* indicate a twofold change. No proteins were statistically significant (FDR < 0.10), and only five proteins displayed a Log2FC > 1. No proteins displayed a Log2FC > 2.

Multidimensional scaling analysis also indicates that samples cluster more closely based on tissues from the same donor rather than on time of preservation (Fig. 5A). There is no distinct clustering of samples based on PMI, although samples from the two donors where the posterior parts were recovered showed higher variance, which was due to increased abundance of Albumin and other blood components (see Discussion). Differential expression analysis did not identify any proteins with differential abundance between the two PMIs.

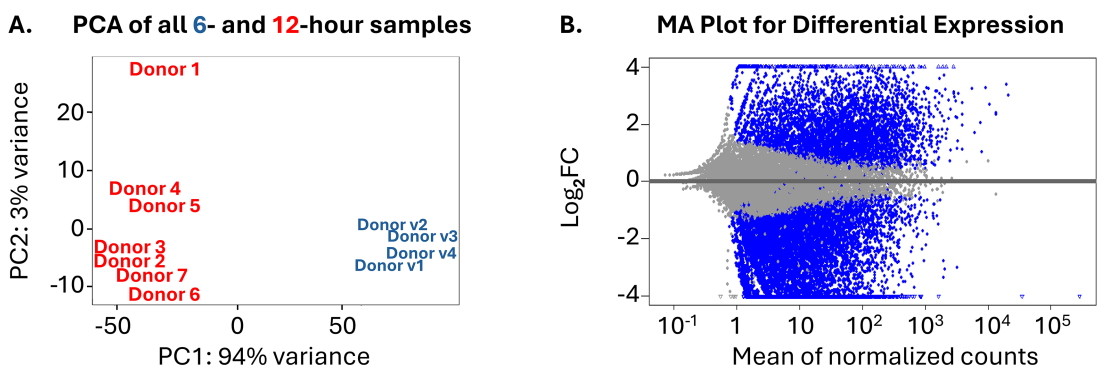

C. Non-Uniform Remodeling of Cell Identity and Stress-induced Pathway Genes

Cell Type	Gene	Log_2FC	*P-adj*
Photoreceptor	RCVRN	-2.54	<0.001
	PDC	-4.06	<0.001
	RHO	-2.22	<0.001
Horizontal Cells	CALB1	-0.54	0.55
Bipolar Cells	VSX2	-0.85	0.70
	TRPM1	-3.32	0.38
Amacrine Cells	PAX6	-0.48	0.32
RGCs	RBPMS	-2.04	<0.001
	CALB2	0.53	0.90
Müller Glia	RLBP1	-0.40	0.86
	PROX1	-0.64	0.30

	Gene	Log_2FC	*P-adj*
House-keeping Markers	GAPDH	0.58	0.58
	PPIB	1.78	0.11
	ACTB	-2.15	0.062
	TUBB	-1.38	0.78
Apoptosis Markers	CASP3	-0.37	0.89
	AIFM1	0.42	0.89
	CRADD	0.82	0.89
	TP53	0.19	0.53
	HTRA1	-1.47	0.08
	CYCS	1.27	0.68
	BAX	0.21	0.90

	Gene	Log_2FC	*P-adj*
Cellular Repair Markers	PARP1	0.68	0.78
	POLR2A	1.90	0.008
	SOD2*	0.84	0.014
	NFE2L2*	0.72	0.002
	GPX4	-0.31	0.89
	DNAJB1	2.30	<0.001
	HSPA1A	0.0	0.0

Figure 6. Meta-analysis of retinal transcripts at six and 12 hours PMI. **(A)** Principal component analysis of samples from the meta-analysis. *Red* = 12-hour samples from this study, and *Blue* = six-hour samples from Voigt et al.,[19] (*v* denotes Voigt). **(B)** MA plot for differentially expressed transcripts. *Blue dots* represent transcripts with adjusted $P < 0.1$. **(C)** Table with selected genes demonstrating heterogeneity of cell identity and stress-induced pathway markers. *Asterisk* denotes potentially interesting changes that did not meet our minimum >1 Log2FC criteria in this study (see Discussion).

Discussion

The consensus among vision researchers is that donor eye tissue is in high demand but in short supply for vision science research.[4–8] Eye banks, meanwhile, have been willing partners in procuring tissue for research.[31] The issue, however, is not the absolute number of donor eyes available but the limited proportion that meet essential criteria. Stamer et al.[32] reported that many researchers request eyes with very short PMI but typically receive tissue with longer preservation times, especially those studying AMD and other retinal diseases. And PMI is only one factor—additional exclusion criteria such as sepsis, chemotherapy, and negative serology results further narrow the pool. As a field, it is therefore to our advantage to expand the donor pool wherever possible, particularly in areas we can control, such as PMI.

Although researchers often request the shortest possible PMI, logistical constraints in the U.S. donation process, outlined in our prior publication,[1] make it difficult to achieve intervals under six hours. As a practical compromise, many collaborators have accepted a 12-hour PMI because it is the shortest interval consistently feasible for tissue procurement. In this study, we therefore examined transcript and protein abundance at 12 hours postmortem and tested the hypothesis that minimal changes occur between 12 and 18 hours, provided the eyes were subjected to ocular cooling after donor death and are refrigerated at 2°C–8°C in moist chambers after recovery in accordance with standard U.S. eye banking practices.

Our results demonstrated 99.9% similarity in the retinal transcriptome and proteome between samples preserved at 12- and 18-hours postmortem. Several groups have successfully isolated high-quality RNA from human retinas with PMIs up to 48 hours.[4–8] At the Veneto Eye Bank Foundation (Venice, Italy), colleagues showed that high-quality RNA can be obtained within 25 hours postmortem.[8] Thus it is not surprising that our study showed minimal changes in transcript abundance in the additional six hours of storage. Likewise, most proteins are known to be stable, and our results show that there is high protein stability in the retina between these two postmortem time points. Additionally, comparisons of semi-tryptic peptide intensities out of the total intensity per sample were compared between the two PMIs and showed no differences (paired *t*-test), suggesting that there was no significant protein degradation. Altogether, our results show that it may be possible to extend the preservation window for donor retinas from 12 to 18 hours, and this can substantially expand the available donor pool. In our prior analysis, this extension was estimated to increase the total number of eligible donor eyes by 92%.[1] Such an increase would accelerate tissue acquisition for retinal research, reduce experimental delays, and do so without compromising data quality.

Our meta-analysis between RNA abundance at six- and 12-hour PMI revealed early postmortem transcriptomic changes that reflect selective cellular vulnerability rather than uniform retinal degradation. The apparent discrepancy between *RBPMS* and *CALB2* further reflects differences in cell-type specificity, as *CALB2* is expressed in both ganglion

Investigative Ophthalmology & Visual Science

and amacrine cells,[33] whereas *RBPMS* is highly restricted to retinal ganglion cells. Pathway analysis further supports this selective vulnerability model, showing decreased abundance of transcripts associated with light detection and retinal homeostasis,[34–36] rather than a global collapse of retinal gene expression. Together, these findings suggest that early postmortem RNA changes are driven by cell-type-specific susceptibility and pathway-specific degradation during early ischemia,[37] followed by relative transcriptomic stabilization at later time points (from 12 to 18 hours).

Although many canonical apoptotic effectors (including *CASP3*, *BAX*, *CYCS*, *AIFM1*, *CRADD*, and *TP53BP2*)[38] showed little or no change in transcript abundance between six and 12 hours, transcripts of *HTRA1*, a mitochondrial-associated serine protease implicated in proteostasis and stress adaptation,[39,40] were significantly reduced, suggesting that specific components of mitochondrial quality control may be lost earlier than the core apoptotic machinery.[41,42]

Several genes involved in oxidative stress defense and cellular damage control exhibited selective regulation. Key regulators of oxidative stress defense showed coordinated but modest changes, with *NFE2L2* and *SOD2* trending upward (~1.5-fold increase, although they did not meet our twofold increase criteria for this study), consistent with an acute response to ischemia-induced reactive oxygen species.[43,44] In contrast, *GPX3*, an extracellular peroxide scavenger, remained stable, indicating that the entire antioxidant pathway is not engaged equally. Strikingly, the molecular chaperone *DNAJB1* and the RNA polymerase II subunit *POLR2A* were strongly upregulated (~4-fold increase), reflecting increased demand for protein quality control and sustained stress-responsive transcription at 12 hours postmortem. Together, this pattern is consistent with a biologically regulated stress-adaptation program in the retina during the first hours after death, rather than passive degradation of the transcriptome.

Prior studies have characterized the number of RNA transcripts in the human retinal transcriptome,[4,45,46] and our results fall within this reported range. Lukowski and colleagues[47] identified 21,990 characterized transcripts across all retinal cell types using the same reference genome annotation, consistent with the 22,446 transcripts found in our study. In addition, we identified 19,797 transcripts with Ensembl gene IDs not yet named in the reference annotation. Many are likely non-coding or antisense RNAs. As transcriptomics advances, these unclassified transcripts will likely be annotated,[48] allowing our data to be reanalyzed with updated references. Comparison of our results with previously published studies indicates that our RNA-seq data are consistent with prior observations and support the conclusion that our dataset is informative and can be a useful tool for researchers.

The lack of significant change in protein abundance between 12- and 18-hour PMI is consistent with prior proteomic studies of kidney, liver, and lung tissue recovered within 24 hours,[49] suggesting that proteins remain relatively stable during this period. In our study, we identified 6109 proteins, substantially more than previous reports of the human retinal proteome.[50,51] For example, Zhang and colleagues[50] identified 3436 proteins in their 2015 study (≈56% of our dataset). Although their eyes were recovered within seven hours postmortem, the retinas were not dissected and frozen until 24–36 hours post donor death, which may have led to protein loss during the additional storage time. In addition, in-gel separation and digestion is less sensitive than our current technique, which may further contribute to the observed differences. A second possibility, one that may also explain the difference in proteins identified in our study compared to amount found in the Zhang study and the 4832 found by Velez and colleagues,[51] is the substantial improvement in mass spectrometry sensitivity (older Orbitrap models and the Agilent 1100 LC systems used in these previous studies compared to the model described in this study).[52,53]

One observation from our study was a noticeable increase in albumin and other blood-related proteins in retinal samples isolated from donor posterior segments. We believe these proteins account for the greater variance observed in the multidimensional scaling analysis (donors 6 and 7, Fig. 5A). These donor tissues differed in that the corneas were excised in the field, with the posterior segments recovered immediately afterward. During cornea excision, blood from surrounding tissue can enter the poles. In contrast, all other eyes in this study were recovered intact and dissected in the laboratory, which minimized additional blood exposure during recovery.

Although blood proteins were elevated in retinas obtained from posterior segments, RNA transcripts for the major plasma proteins—albumin, globulins, and fibrinogen—were not detected in any donor sample. Because these proteins are likely synthesized in the liver and bone marrow and transported to the retina, the absence of their transcripts is not unexpected.[54,55] This variability in blood protein content, driven by recovery technique and logistics, should be taken into account when requesting retinal tissues for proteomic studies.

The results of our study also provide researchers with a valuable tool to examine transcript and protein abundance in the human retina for up to 18 hours postmortem. An example of the dataset's utility is during the experimental design phase of a project where selection of molecular markers is required. For instance, those studying Müller glia cells may choose RLBP1 as a protein marker given its high abundance, whereas those examining gene transcripts may elect to use PROX1, as its transcript levels remain high at 18 hours postmortem. This example highlights the practical value of the dataset, which can support not only current research needs but also future studies in ways we cannot yet anticipate.

In both our transcriptomic and proteomic analyses (Figs. 3, 5), we observed that samples consistently clustered by donor rather than by PMI, indicating that inter-individual biological variability outweighed any molecular differences attributable to the 12- versus 18-hour time points. This pattern reflects a well-recognized challenge in human tissue research: each donor presents a unique combination of genetic background, medical history, lifestyle factors, and environmental exposures that can introduce substantial variation into omics datasets. Our study design sought to minimize these confounding variables by using paired right and left eyes from the same donor, allowing each individual to serve as their own biological control. By comparing tissues collected from the same donor at two PMIs, we effectively controlled for genetic and donor-specific influences, thereby isolating PMI as the primary variable of interest. The fact that paired samples cluster together while failing to separate by PMI reinforces our conclusion that molecular changes between 12 and 18 hours postmortem are minimal and underscores the importance of careful study design when using human donor tissues for molecular analyses.

Investigative Ophthalmology & Visual Science

Study Limitations

Although our meta-analysis revealed biologically plausible patterns, its interpretation is necessarily constrained by substantial methodological differences between the contributing datasets. The studies differed in RNA extraction protocols, library preparation methods, sequencing platforms, and donor sources, making it difficult to fully disentangle technical and inter-individual variability from true PMI-dependent effects. For this reason, we view the meta-analysis primarily as a hypothesis generating tool, whereas our within-donor experimental design provides a more rigorous framework for quantifying postmortem transcriptomic changes. Definitive validation of the observed trends will require replication using the standardized experimental and analytical pipeline established here.

The main study is itself limited by the range of PMIs examined, which was restricted to 12–18 hours. However, our meta-analysis of the six-hour samples along with previous studies comparing live and postmortem retina samples[56] suggests that there can be pronounced transcriptomic remodeling that occurs during earlier postmortem times. Building on these findings, future work will extend our sampling to earlier PMIs to capture the initial ischemic response, as well as to later PMIs to better define downstream effects on protein abundance and tissue function. Nevertheless, the present dataset already offers actionable insight that can immediately support broader use of donor retinas for research and therefore stands as a meaningful contribution on its own.

Conclusions

Our controlled study of donor eyes with ocular cooling after death shows that transcript and protein abundance remain essentially unchanged between 12 and 18 hours postmortem. Extending the current 12-hour cutoff to 18 hours provides a scientifically sound and logistically practical approach to accessing more donor eyes for biomedical research that better aligns with the logistical realities of tissue donation and eye banking.

Acknowledgments

The authors thank the organ, eye, and tissue donors and their families for their generous gift of tissues that made this work possible.

Supported by a research grant from the Eppley Foundation for Research to K.D.T. Mass spectrometric analysis was performed by the OHSU Proteomics Shared Resource with partial support from NIH core grants P30EY010572, P30CA069533, and S10 OD028533.

Availability of Data and Materials: The RNA-seq data has been uploaded to the SRA database. All samples can be accessed by visiting: https://trace.ncbi.nlm.nih.gov/Traces/?view=study&acc=SRP630536. **SRA:** SRP630536, **BioProject:** PRJNA1337673. The mass spectrometry proteomics data have been deposited to the ProteomeXchange Consortium via the PRIDE[57] partner repository with the dataset identifier PXD068030.

Disclosure: **C.A. Easton**, VisionGift (E); **P.A. Wilmarth**, OHSU (E); **M. Criss**, Floragenex, Inc. (E); **K. Kim**, OHSU (E); **A.P. Reddy**, OHSU (E); **S. Tanne**, VisionGift (E); **J.Q. Boone**, Floragenex, Inc. (E); **K.D. Tran**, VisionGift (E)

References

1. Straiko MMW, Ellison MS, Patzer C, Westrick K, Tran KD. Provision of human ocular tissue for biomedical research: trends, limitations, and potential solutions from an eye bank. *Sci Rep*. 2025;15(1):7958.
2. Kallestad L, Blackshaw S, Khalil AM, Palczewski K. Tissue- and species-specific patterns of RNA metabolism in postmortem mammalian retina and retinal pigment epithelium. *Sci Rep*. 2019;9(1):14821.
3. Malik KJ, Chen CD, Olsen TW. Stability of RNA from the retina and retinal pigment epithelium in a porcine model simulating human eye bank conditions. *Invest Ophthalmol Vis Sci*. 2003;44:2730–2735.
4. Cai H, Fields MA, Hoshino R, Priore LV. Effects of aging and anatomic location on gene expression in human retina. *Front Aging Neurosci*. 2012;4:8.
5. Kim BJ, Sprehe N, Morganti A, Wordinger RJ, Clark AF. The effect of postmortem time on the RNA quality of human ocular tissues. *Mol Vis*. 2013;19:1290–1295.
6. Young TL, Hawthorne F, Feng S, et al. Whole genome expression profiling of normal human fetal and adult ocular tissues. *Exp Eye Res*. 2013;116:265–278.
7. Montanini L, Ferrari S, Crafa P, et al. Human RNA integrity after postmortem retinal tissue recovery. *Ophthalmic Genet*. 2013;34(1-2):27–31.
8. Parekh M, Montanini L, Crafa P, et al. A validated biorepository of retina and choroid tissues for gene expression studies. *Biopreserv Biobank*. 2014;12:255–258.
9. Kim SU, Takahashi H. Tissue culture study of adult human retina neurons. *Invest Ophthalmol Vis Sci*. 1988;29:1372–1379.
10. Eye Bank Association of America. *2017 Medical Standards*. 2017.
11. Provis JM, Dubis AM, Maddess T, Carroll J. Adaptation of the central retina for high acuity vision: cones, the fovea and the avascular zone. *Prog Retin Eye Res*. 2013;35:63–81.
12. Hoshino A, Ratnapriya R, Brooks MJ, et al. Molecular anatomy of the developing human retina. *Dev Cell*. 2017;43:763–779.
13. Fletcher EL, Jobling AI, Greferath U, et al. Studying age-related macular degeneration using animal models. *Optom Vis Sci*. 2014;91:878–886.
14. Pennesi ME, Neuringer M, Courtney RJ. Animal models of age related macular degeneration. *Mol Aspects Med*. 2012;33:487–509.
15. Hahn J, Monavarfeshani A, Qiao M, et al. Evolution of neuronal cell classes and types in the vertebrate retina. *Nature*. 2023;624(7991):415–424.
16. Peichl L. Diversity of mammalian photoreceptor properties: adaptations to habitat and lifestyle? *Anat Rec A Discov Mol Cell Evol Biol*. 2005;287:1001–1012.
17. Kim US, Mahroo OA, Mollon JD, Yu-Wai-Man P. Retinal ganglion cells-diversity of cell types and clinical relevance. *Front Neurol*. 2021;12:661938.
18. Love MI, Huber W, Anders S. Moderated estimation of fold change and dispersion for RNA-seq data with DESeq2. *Genome Biol*. 2014;15:550.
19. Voigt AP, Mullin NK, Whitmore SS, et al. Human photoreceptor cells from different macular subregions have distinct transcriptional profiles. *Hum Mol Genet*. 2021;30:1543–1558.
20. Wilmarth PA, Riviere MA, David LL. Techniques for accurate protein identification in shotgun proteomic studies of human, mouse, bovine, and chicken lenses. *J Ocul Biol Dis Infor*. 2009;2:223–234.
21. Eng JK, Jahan TA, Hoopmann MR. Comet: an open-source MS/MS sequence database search tool. *Proteomics*. 2013;13:22–24.

22. Robinson MD, Oshlack A. A scaling normalization method for differential expression analysis of RNA-seq data. *Genome Biol*. 2010;11(3):R25.
23. Robinson MD, McCarthy DJ, Smyth GK. edgeR: a Bioconductor package for differential expression analysis of digital gene expression data. *Bioinformatics*. 2010;26:139–140.
24. Anderson DE, Holstein SA, Kedar S. Visual pathway degeneration in chemotherapy-related neurotoxicity: a review and directions for future research. *Neuroophthalmology*. 2020;44:139–147.
25. Schwanhausser B, Busse D, Li N, et al. Global quantification of mammalian gene expression control. *Nature*. 2011;473(7347):337–342.
26. Clark MB, Johnston RL, Inostroza-Ponta M, et al. Genome-wide analysis of long noncoding RNA stability. *Genome Res*. 2012;22:885–898.
27. Mi H, Muruganujan A, Huang X, et al. Protocol Update for large-scale genome and gene function analysis with the PANTHER classification system (v.14.0). *Nat Protoc*. 2019;14:703–721.
28. Thomas PD, Ebert D, Muruganujan A, Mushayahama T, Albou LP, Mi H. PANTHER: making genome-scale phylogenetics accessible to all. *Protein Sci*. 2022;31:8–22.
29. Xi Z, Ozturk BE, Johnson ME, Turunc S, Stauffer WR, Byrne LC. Quantitative single-cell transcriptome-based ranking of engineered AAVs in human retinal explants. *Mol Ther Methods Clin Dev*. 2022;25:476–489.
30. Rodriguez AR, de Sevilla Muller LP, Brecha NC. The RNA binding protein RBPMS is a selective marker of ganglion cells in the mammalian retina. *J Comp Neurol*. 2014;522:1411–1443.
31. Corcoran KP. Accessibility to and quality of human eye tissue for research: a cross-sectional survey of ARVO members - EBAA commentary. *Invest Ophthalmol Vis Sci*. 2018;59:4793–4795.
32. Stamer WD, Williams AM, Pflugfelder S, Coupland SE. Accessibility to and quality of human eye tissue for research: a cross-sectional survey of ARVO members. *Invest Ophthalmol Vis Sci*. 2018;59:4783–4792.
33. Kantor O, Mezey S, Adeghate J, et al. Calcium buffer proteins are specific markers of human retinal neurons. *Cell Tissue Res*. 2016;365:29–50.
34. Xiong B, Bellen HJ. Rhodopsin homeostasis and retinal degeneration: lessons from the fly. *Trends Neurosci*. 2013;36:652–660.
35. Hussey KA, Hadyniak SE, Johnston RJ, Jr. Patterning and development of photoreceptors in the human retina. *Front Cell Dev Biol*. 2022;10:878350.
36. Abbas F, Becker S, Jones BW, et al. Revival of light signalling in the postmortem mouse and human retina. *Nature*. 2022;606(7913):351–357.
37. Palmhof M, Frank V, Rappard P, et al. From ganglion cell to photoreceptor layer: timeline of deterioration in a rat ischemia/reperfusion model. *Front Cell Neurosci*. 2019;13:174.
38. Mustafa M, Ahmad R, Tantry IQ, et al. Apoptosis: a comprehensive overview of signaling pathways, morphological changes, and physiological significance and therapeutic implications. *Cells*. 2024;13(22):1838.
39. Gerhardt MJ, Marsh JA, Morrison M, et al. ER stress-induced aggresome trafficking of HtrA1 protects against proteotoxicity. *J Mol Cell Biol*. 2017;9:516–532.
40. Jones A, Kumar S, Zhang N, et al. Increased expression of multifunctional serine protease, HTRA1, in retinal pigment epithelium induces polypoidal choroidal vasculopathy in mice. *Proc Natl Acad Sci USA*. 2011;108:14578–14583.
41. Produit-Zengaffinen N, Pournaras CJ, Schorderet DF. Retinal ischemia-induced apoptosis is associated with alteration in Bax and Bcl-x(L) expression rather than modifications in Bak and Bcl-2. *Mol Vis*. 2009;15:2101–2110.
42. Eckl EM, Ziegemann O, Krumwiede L, Fessler E, Jae LT. Sensing, signaling and surviving mitochondrial stress. *Cell Mol Life Sci*. 2021;78:5925–5951.
43. Wei Y, Gong J, Yoshida T, et al. Nrf2 has a protective role against neuronal and capillary degeneration in retinal ischemia-reperfusion injury. *Free Radic Biol Med*. 2011;51:216–224.
44. Liu Y, Tang L, Chen B. Effects of antioxidant gene therapy on retinal neurons and oxidative stress in a model of retinal ischemia/reperfusion. *Free Radic Biol Med*. 2012;52:909–915.
45. Riepe TV, Stemerdink M, Salz R, et al. A proteogenomic atlas of the human neural retina. *Front Genet*. 2024;15:1451024.
46. Li M, Jia C, Kazmierkiewicz KL, et al. Comprehensive analysis of gene expression in human retina and supporting tissues. *Hum Mol Genet*. 2014;23:4001–4014.
47. Lukowski SW, Lo CY, Sharov AA, et al. A single-cell transcriptome atlas of the adult human retina. *EMBO J*. 2019;38(18):e100811.
48. Amaral P, Carbonell-Sala S, De La, Vega FM, et al. The status of the human gene catalogue. *Nature*. 2023;622(7981):41–47.
49. Kocsmar E, Schmid M, Cosenza-Contreras M, et al. Proteome alterations in human autopsy tissues in relation to time after death. *Cell Mol Life Sci*. 2023;80(5):117.
50. Zhang P, Dufresne C, Turner R, et al. The proteome of human retina. *Proteomics*. 2015;15:836–840.
51. Velez G, Machlab DA, Tang PH, et al. Proteomic analysis of the human retina reveals region-specific susceptibilities to metabolic- and oxidative stress-related diseases. *PloS one*. 2018;13(2):e0193250.
52. Son A, Kim W, Park J, et al. Mass spectrometry advancements and applications for biomarker discovery, diagnostic innovations, and personalized medicine. *Int J Mol Sci*. 2024;25:9880.
53. Wang Z, Kavdia K, Dey KK, et al. High-throughput and deep-proteome profiling by 16-plex tandem mass tag labeling coupled with two-dimensional chromatography and mass spectrometry. *J Vis Exp*. 2020;18(162):e61684. doi:10.3791/61684.
54. Lucas D. Structural organization of the bone marrow and its role in hematopoiesis. *Curr Opin Hematol*. 2021;28(1):36–42.
55. Kur J, Newman EA, Chan-Ling T. Cellular and physiological mechanisms underlying blood flow regulation in the retina and choroid in health and disease. *Prog Retin Eye Res*. 2012;31:377–406.
56. Yang L, Tao Y, Pan Q, et al. A scRNA-seq reference contrasting living and early post-mortem human retina across diverse donor states. *Hum Genomics*. 2025;19:81.
57. Perez-Riverol Y, Bandla C, Kundu DJ, et al. The PRIDE database at 20 years: 2025 update. *Nucleic Acids Res*. 2025;53(D1):D543–D553.

Investigative Ophthalmology & Visual Science